Numerical simulation of two-dimensional multiple scattering of sound by a large number of circular cylinders

Adrien Rohfritsch,[a] Jean-Marc Conoir, Régis Marchiano, and Tony Valier-Brasier
Sorbonne Université, Centre National de la Recherche Scientifique, UMR 7190, Institut Jean Le Rond d'Alembert, Paris, F-75005, France

(Received 25 February 2019; revised 17 April 2019; accepted 11 May 2019; published online 7 June 2019)

The purpose of this article is to present an innovative resolution method for investigating problems of sound scattering by infinite cylinders immersed in a fluid medium. The study is based on the analytical solution of multiple scattering, where incident and scattered waves are expressed in cylindrical harmonics. This modeling leads to dense linear systems, which are made sparse by introducing a *cutoff radius* around each particle. This cutoff radius is deeply studied and quantified. Numerical resolution is performed using parallel computing methods designed to solve very large sparse linear systems. Comparisons with direct calculations made with another numerical software and homogenization techniques follow and show good agreement with the implemented method. The last part is dedicated to a comparison between the propagation of waves in a circular cluster made of a random distribution of cylinders and the propagation in the corresponding homogenized cluster where the multiple scattering formalism is combined with a statistical analysis to provide an effective medium. https://doi.org/10.1121/1.5110310

[NAG] Pages: 3320–3329

I. INTRODUCTION

Multiple scattering of waves is a general problem that occurs in many fields of physics. Both the acoustical and electromagnetical physics communities have problems of great interest that deal with multiple scattering such as the characterization of effective parameters of heterogeneous media or phononic crystals, for example.

Here, we present a study of scattering by infinite parallel cylinders. The model used in this paper to describe the wave propagation through a cluster of cylinders was first presented by Zàviška.[1] It is an analytical model that leads to writing the solution in an implicit way through a linear system of great size, which increases with frequency and the number of cylinders. In view of the difficulty to resolve this dense linear system, two strategies have emerged.

The first is based on statistical tools applied to the expression of the total acoustical field, leading to the calculation of statistical quantities, for instance, self-energy or effective wave numbers. As a partial overview of notable papers based on the multiple scattering model, one can note, for instance, Bose *et al.*[2] for the study of wave propagation in fiber-reinforced composites. This study is based on the quasi-crystalline approximation, introduced by Lax,[3] that gives exact results for crystal lattices. Later on, Varadan *et al.*[4] generalized this case to arbitrary shaped scatterers. Le Bas *et al.*[5] have introduced the *S*-matrix to study the resonant interaction between cylinders. More recently, a paper by Linton and Martin[6] deals with the second-order corrections of effective wave numbers in elastic media, and derives Twersky's expressions to criticize their relevance. Later, Norris and Conoir[7] performed the calculation of effective wave numbers up to fourth order. All these analytical models based on statistical tools are intrinsically limited by the concentration and the geometry of the cluster of cylinders, which is often a half-plane or a slab.

The second strategy emerged at the beginning of the 1970s. At that time, new numerical methods were available, offering possibilities to resolve multiple scattering problems. First, numerical studies were conducted with two cylinders[8,9] or circular arrays of cylinders around a point source.[10] Over the years, iterative methods have been developed to calculate the exact solution by using parallel computing. Several methods were designed to resolve problems with particular geometry such as lattices or uniform distributions in a slab. A wide overview of these numerical methods has been presented recently by Amirkulova and Norris.[11] Among all these methods, the fast multipole method (FMM), proposed by Greengard and Rokhlin[12] for particle simulations, was later extended for acoustic and electromagnetic scattering calculations. It is worth noting that many efforts have been put on FMM in three-dimensional (3D) multiple scattering problems taking into account a large number of spherical particles. More details can be obtained by referring to Refs. 13 and 14 and the book written by Gumerov and Duraiswami[15] presenting an up-to-date discussion of the FMM, including different expansions and convergence analyses. Surprisingly enough, the FFM has received less attention in two dimensions (2D), where it has been implemented by Zhang and Li[16] with a special attention to phononic crystals.

The objective of this paper is to develop a numerical method of resolution based on the equations of the multiple scattering theory. We focus on demonstrating how the number of non-zero matrix entries can be decreased by introducing a cutoff radius around each cylinder. This radius makes the system sparse and easier to solve using relevant iterative methods. For implementation, we use a library developed to

[a]Electronic mail: adrien.rohfritsch@sorbonne-universite.fr

 0001-4966/2019/145(6)/3320/10/$30.00

solve large linear sparse systems (Portable, Extensible Toolkit for Scientific Computation, PETSC[17–19]). This library is used with message passing interface (MPI) architecture, which is the key tool to ensure the scalability of the resolution. Indeed, the same implementation works as well on a computer of 24 processors as on a computer of 512 processors; there is no limit to the size of the problem. This implementation allows computation of the most general multiple scattering cases: any number of scatterers, any number of modes (i.e., any frequency) can be treated, as well as any random geometry (with any concentration) or any cylinder type and incident wave type (plane wave, point source, etc.). Validation tests open a comparison between homogeneous (statistical) predictions and our resolution (called MuScat in this paper, for multiple scattering). The last part is dedicated to the study of the directivity diagram of a circular cluster of randomly distributed cylinders. In this case computations are performed with matrices of size $N \times N = 85\,100 \times 85\,100$ on a computer of 64 processors.

II. THEORETICAL MODEL

This section is dedicated to the presentation of the model of multiple scattering of sound waves in 2D. The acoustic pressure is written $pe^{-i\omega t}$, and satisfies the Helmholtz equation

$$\Delta p + k^2 p = 0, \tag{1}$$

where $k = \omega/c$ is the wave number and c is the speed of sound in the host medium. For the sake of simplicity, the time dependence $e^{-i\omega t}$ is omitted throughout the text. The pressure field is expressed in the coordinate system (r,θ) which is linked to an arbitrary center O. In 2D, any wave can be decomposed in the basis of the cylindrical harmonics, and that gives for the incident pressure p_0,

$$p_0(\mathbf{r}) = \sum_{n=-\infty}^{+\infty} b_n J_n(kr) e^{in\theta}, \tag{2}$$

where coefficients b_n are the amplitudes of each mode and J_n is the Bessel function of order n. For instance, for a plane wave propagating along the x axis, the coefficients b_n are $(-i)^n$. The total sound field in a particular configuration of N_s scatterers can be expressed as the sum of the incident wave and the waves scattered by all scatterers

$$p(\mathbf{r}) = p_0(\mathbf{r}) + \sum_{j=1}^{N_s} p_s^{(j)}(\mathbf{r_j}). \tag{3}$$

Figure 1 indicates the notations used in the following, illustrating that our resolution is not limited to a unique type of cylinder. Equation (3) expresses waves diverging from each cylinder with respect to their own coordinate systems $\mathbf{r_j} = (r_j \cos\,\theta_j, r_j \sin\,\theta_j)^t$. It follows that

$$p_s^{(j)}(\mathbf{r_j}) = \sum_{n=-\infty}^{+\infty} A_n^{(j)} H_n^{(1)}(k\mathbf{r_j}) e^{in\theta_j}, \tag{4}$$

where $H_n^{(1)}$ is the Hankel function of the first kind and order n, and the scattering amplitudes $A_n^{(j)}$ are the unknowns of the problem. Every scattered wave becomes an incident wave for the other cylinders. Hence, the incident wave on scatterer j, $p_{\text{inc}}^{(j)}$, is written as

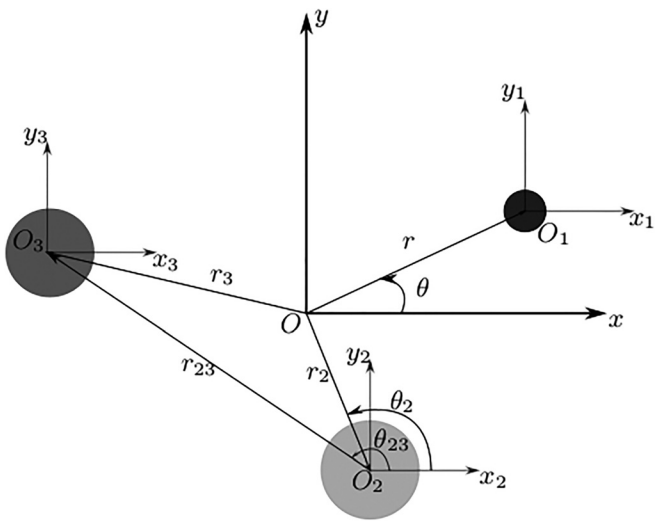

FIG. 1. Arbitrary planar configuration of parallel cylinders.

$$p_{\text{inc}}^{(j)} = p_0^{(j)} + \sum_{\substack{k=1 \\ k\neq j}}^{N_s} \sum_{n=-\infty}^{+\infty} A_n^{(k)} H_n^{(1)}(kr_k) e^{in\theta_k}. \tag{5}$$

Using the addition theorem,[20] cylindrical harmonics with origin at r_p can be expressed as a sum of cylindrical harmonics with origin at r_q thanks to the relations

$$\begin{cases} z_n(kr_p)e^{in\theta_p} = \displaystyle\sum_{\nu=-\infty}^{+\infty} z_{n-\nu}(kr_{pq}) e^{i(n-\nu)\theta_{pq}} J_\nu(kr_q) e^{i\nu\theta_q}, \\ \qquad\qquad \text{if } r_q < r_{pq}, \\ z_n(kr_p)e^{in\theta_p} = \displaystyle\sum_{\nu=-\infty}^{+\infty} J_{n-\nu}(kr_{pq}) e^{i(n-\nu)\theta_{pq}} z_\nu(kr_q) e^{i\nu\theta_q}, \\ \qquad\qquad \text{if } r_q > r_{pq}, \end{cases} \tag{6}$$

where z_n can either be J_n or $H_n^{(1)}$, and $\mathbf{r_{pq}} = \mathbf{r_p} - \mathbf{r_q}$. Substituting Eq. (6) in Eq. (5) yields

$$p_{\text{inc}}^{(j)} = \sum_{\nu=-\infty}^{+\infty} \sum_{n=-\infty}^{+\infty} \left[N_{\nu n}^{(0j)} b_n + \sum_{\substack{k=1 \\ k\neq j}}^{N_s} M_{\nu n}^{(kj)} A_n^{(k)} \right] J_\nu(kr_j) e^{i\nu\theta_j}, \tag{7}$$

with

$$\begin{cases} M_{\nu n}^{(kj)} = H_{\nu-n}^{(1)}(kr_{kj}) e^{i(\nu-n)\theta_{kj}}, \\ N_{\nu n}^{(0j)} = J_{\nu-n}(kr_{0j}) e^{i(\nu-n)\theta_{0j}}. \end{cases} \tag{8}$$

Taking into account the scattering coefficients $T_n^{(j)}$ of the $\mathbb{T}^{(j)}$ matrix, it follows from Eqs. (4) and (7) that we have

$$A_n^{(j)} = T_n^{(j)} \left[\sum_{n=-\infty}^{+\infty} N_{\nu n}^{(0j)} b_n + \sum_{\substack{k=1 \\ k\neq j}}^{N_s} \sum_{n=-\infty}^{+\infty} M_{\nu n}^{(kj)} A_n^{(k)} \right]. \tag{9}$$

For circular cylinders, the $\mathbb{T}^{(j)}$ matrix is diagonal with coefficients $\mathbb{T}^{(j)}_{np} = T^{(j)}_n \delta_{np}$. Its coefficients are calculated imposing continuity of displacements and stress vector at the boundaries of the cylinders and fluid. For instance, they are for the case of a soft cylinder of radius a,

$$T^{(j)}_n = -\frac{J_n(ka)}{H^{(1)}_n(ka)}. \tag{10}$$

Note that the cylinders considered in this paper are either soft cylinders (see Sec. IV A) or elastic cylinders (see all other sections), and their elastic properties can be chosen by changing $T^{(j)}_n$.[21,22] Equation (9) can be formulated in a vectorial way as follows:

$$\mathbf{A}^{(j)} = \mathbb{T}^{(j)} \left[\mathbb{N}^{(0j)}\mathbf{b} + \sum_{\substack{k=0 \\ k\neq j}}^{N_s} \mathbb{M}^{(jk)}\mathbf{A}^{(k)} \right]. \tag{11}$$

If the modal sum is truncated at order N_m, Eq. (11) involves $2N_m - 1$ equations for each scatterer. The total size of the system is then $N \times N$ with $N = N_s \times (2N_m - 1)$, and can be written as

$$[\mathcal{I} - \mathcal{T}\mathcal{M}]\mathbf{A} = \mathcal{T}\mathbf{E}, \tag{12}$$

with the following notations

$$\begin{cases} \mathbf{A} = (\mathbf{A}^{(1)}, \mathbf{A}^{(2)}, \ldots, \mathbf{A}^{(N_s)})^t, \\ \mathbf{E}_p = \mathbb{N}^{(0p)}\mathbf{b}, \\ \mathcal{T}_{pq} = \mathbb{T}^{(p)}\delta_{pq}, \\ \mathcal{M}_{pq} = \mathbb{M}^{(pq)}(1-\delta_{pq}). \end{cases} \tag{13}$$

Solving the linear system (12) gives all the amplitudes of the waves scattered by the N_s arbitrarily distributed scatterers. The calculation of the inverse of the matrix $[\mathcal{I} - \mathcal{T}\mathcal{M}]$ is a very demanding process because of its large size and the fact that it is a dense system. Section III is devoted to our numerical strategy and method to resolve it.

III. NUMERICAL METHOD

A. Truncation of the modal sum

The matrix of the linear system (12) is complex-valued, dense, of size $N \times N$ with $N = N_s \times (2N_m - 1)$. The first parameter to set is the number of modes to take into account (N_m), which increases as a function of frequency. A common empirical approach to truncate the modal sum is to choose N_m as[23]

$$N_m = \left[ka + (1/(2\sqrt{2}) \ln (2\sqrt{2}\pi ka\epsilon^{-1}))^{2/3} + 1 \right],$$

where a is the radius of the scatterers, $[x]$ is the integer part of a real number x, and ϵ is the desired error bound on the scattering amplitudes. This threshold can be insufficient for configurations with very close cylinders. Valier-Brasier and Conoir[24] recently showed that a large number of modes has to be taken into account in the case of resonant interactions between close scatterers (for instance, bubbles or soft cylinders). In this paper, to be sure to converge, we chose to calculate the number N_m by resolving a two cylinder problem with an in-between distance equal to the minimal distance between cylinders in the distribution we want to focus on. Then, starting with $N_m = 1$ and increasing it more and more, calculation stops when $|A^{1,2}_{N_m+1}| < \text{tol}$ and $|A^{1,2}_{N_m+2}| < \text{tol}$ simultaneously; tol parameter is set at 10^{-6}.

B. From dense to sparse systems

If the size of the matrix becomes large, there is a possible overflow of the memory space.

A close look at the matrix shows that each line corresponds to the interaction of a scatterer with all other scatterers. But these interactions clearly become smaller as the distance between them increases; the wave scattered by one cylinder does not contribute to the field incoming upon on another scatterer located at a very long distance. This leads to the idea of a cutoff radius (D) around each scatterer that represents the horizon beyond which cylinders do not interact anymore. This radius is related to the quantities of the problem: the wavelength of the source, the concentration of cylinders, the geometry of the cluster, and the elastic properties of the cylinders being the most important.

Imposing this cutoff radius leads to a new problem to solve, written as

$$[\mathcal{I} - \mathcal{T}\tilde{\mathcal{M}}]\tilde{\mathbf{A}} = \mathcal{T}\mathbf{E}, \tag{14}$$

with $\tilde{\mathcal{M}}$ the new sparse matrix of the problem and $\tilde{\mathbf{A}}$ the new amplitude vector.

Now that a new sparse problem has been constructed, one has to know how to resolve it.

C. Iterative methods designed to work through MPI

To resolve such huge sparse linear systems, direct methods are known to be inefficient because of their time and memory costs; for instance, the Gauss-Jordan method requires $\mathcal{O}(N^3)$ operations and lower-upper (LU) decomposition $2N^3/3$.[11] Iterative methods are then more suitable. Those based on Krylov subspaces have concentrated a lot of effort over the last two decades.[23,25,26] A set of these methods is computed in PETSC's library,[17–19] which we chose here to perform the resolution.

This library works using MPI. This parallel computing architecture is characterized by the fact that each processor has its own memory storage. Data communication is performed from one processor to another. An important advantage of this architecture is the scalability of the resolution. Indeed, after implementing the resolution on a computer of 64 processors, one can immediately launch it on computers of 24 or 512 processors without any difficulty, and therefore increase the maximum size of problems that can be resolved.

For each matrix type, a particular iterative method has to be chosen because it has to take into account the global and local properties of the matrix $[\mathcal{I} - \mathcal{T}\tilde{\mathcal{M}}]$. In our case, it

is a complex-valued asymmetrical matrix. Many studies are limited to cases with periodic lattices, for which the problem is easier to solve. For instance, Biwa *et al.*[27] focused on the propagation of shear waves in periodic lattices (even though they presented the general model), studying propagation in composite media. More recently, Amirkulova and Norris[11] compared the LAPACK and TOEPLITZ libraries, and treated problems of phononic crystals composed of a few hundred cylinders.

The objective of the study here is to resolve the problem for the most general case for which the matrix does not have particular symmetries. Three of the suitable methods for such matrices were studied in terms of convergence rate: stabilized version of BiConjugate gradient (BCGS), generalized minimal residual method (GMRES), and left conjugate direction (LCD). The preconditioner block Jacobi is chosen for the three methods. Two comparisons are presented in Fig. 2 for a random distribution of 480 steel cylinders with a concentration of $\phi = 8\%$, the time needed to reach converge (above) and number of iterations to converge (below). Here, the sparsity of the system is such that ∼20% of the interactions between scatterers are taken into account; all cylinders interact with the closest 20% cylinders.

GMRES is chosen to perform all the simulations throughout this paper because of its better resolution speed in a classical frequency range. One can note that the BCGS method gives close results in terms of time, and better results in terms of number of iterations (but each iteration takes more time).

Numerical methods for solving large linear sparse systems are now well established.

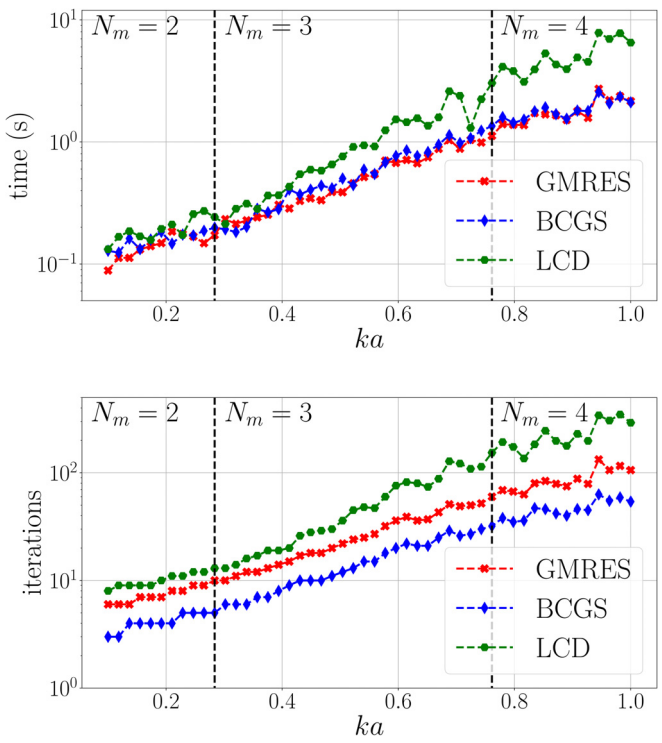

FIG. 2. (Color online) Comparison between three iterative methods (GMRES, BCGS, and LCD) in terms of convergence time (top) and number of iterations (bottom). Calculations are performed on 480 steel cylinders of radius $a = 1$ mm randomly distributed in water with a global concentration of $\phi = 8\%$.

D. Controlling the error introduced by the cutoff radius

Now that one knows how to make the system sparse and an efficient method to solve sparse asymmetrical systems has been chosen, the error created by the introduction of the cutoff radius has to be quantified; the question is now how to choose D and what error is created by this choice.

This error is evaluated through the error made on the acoustic field (which is directly related to the amplitudes themselves, but closest to physical considerations). Several simulations are performed on circular random distributions of steel and epoxy cylinders in water. This geometry is chosen because it minimises the number of scatterers close to the domain boundaries. To cancel boundary effects, no cutoff radius is applied to cylinders too close from the boundary (i.e., for which the exclusion circle is totally included in the cluster).

The radius of each distribution is six times larger than the wavelength of the incident field, which is a plane wave. The error created by the cutoff radius is calculated by the relation

$$\Delta_E = \sqrt{\left(\frac{\sum_{r}^{N_r} \sum_{\theta}^{N_\theta} |p(r,\theta) - \tilde{p}(r,\theta)|^2}{\sum_{r}^{N_r} \sum_{\theta}^{N_\theta} |p(r,\theta)|^2} \right)}, \tag{15}$$

where $p(r,\theta)$ is the exact pressure field (calculated by resolving the dense system) and $\tilde{p}(r,\theta)$ is the approximate pressure field. N_r is the number of sampling points in the radial direction, and N_θ is the number of sampling points in the angular direction. These two parameters, as soon as they are taken large enough (few tens by wavelengths, in our case) do not impact the value of Δ_E. Here, we chose to impose $\Delta_E = 10\%$. The calculations are performed for different frequencies and concentrations in such a way that the dense version of the matrix can fit in the memory of a 125 Gb computer. The maximum values of the cutoff radius normalized by the wavelength to obtain an error equal to 10% are given in Fig. 3 for steel cylinders and epoxy cylinders as a function of $\phi \in [5\%,20\%]$ and the frequency parameter $ka \in [0.1,1.0]$. Twenty-four points have been calculated in frequency and 12 in concentration.

This surface can be fitted by a function of two parameters. For each study, one can then determine which cutoff radius should be imposed in order to have a *tolerable* error. Writing $\tilde{D}(ka,\phi) = D(ka,\phi)/\lambda$ as the products of two polynomials of degree deg,

$$\begin{aligned} \tilde{D}(ka,\phi) &= \left[\sum_{i=0}^{\deg} a_i (ka)^i \right] \left[\sum_{j=0}^{\deg} b_j \phi^j \right] \\ &= \sum_{i=0}^{\deg} \sum_{j=0}^{\deg} c_l (ka)^i \phi^j, \quad \text{with } l = j + i\,\deg, \end{aligned} \tag{16}$$

one can use a least square method to determine appropriate values for coefficients. In the case of steel cylinders,

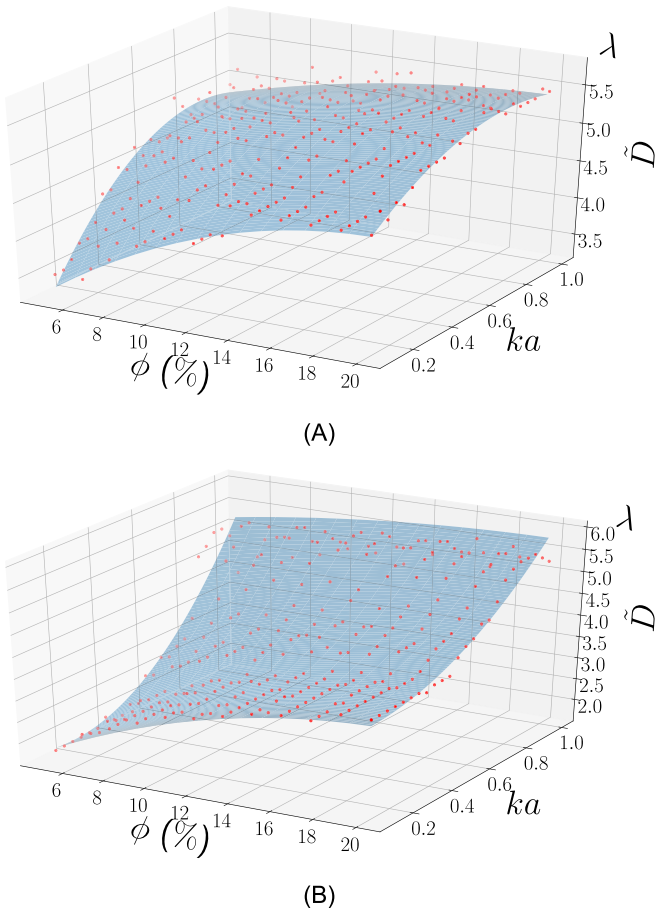

FIG. 3. (Color online) Maximum values for cutoff radius for which the error is $\Delta_E = 10\%$ as a function of frequency and concentration for two types of elastic cylinders: (A) steel ($\rho_c = 7850\,\mathrm{kg\,m^{-3}}$, $c_L = 5700\,\mathrm{m\,s^{-1}}$, $c_T = 3000\,\mathrm{m\,s^{-1}}$) and (B) epoxy ($\rho_c = 1200\,\mathrm{kg\,m^{-3}}$, $c_L = 1500\,\mathrm{m\,s^{-1}}$, $c_T = 800\,\mathrm{m\,s^{-1}}$).

Fig. 3(A) shows that $\tilde{D}$ behavior is quite smooth. In this case, interpolated surface gives good approximation with $\deg = 2$. Coefficients are given in Table I. In the case of epoxy cylinders [Fig. 3(B)], an elastic resonance around $ka = 0.88$ makes the behavior much more complicated, for which $\deg = 4$ has to be chosen in order to get a correct interpolation. For the sake of legibility, the 23 coefficients for this second surface are not given in the text.

We chose here to link the dimension of cutoff radius to the wavelength. Other lengths can be chosen, such as radius a, elastic mean free path l_e, cluster size R_c, or even mean distance between cylinders d (depending on the concentration). The elastic mean free path can appear as a very relevant quantity because of its strong dependency on frequency and concentration, but there are two main problems with it. The first problem is related to cylinder resonances. The second problem is linked with the fact that, outside of low concentration regimes, it is difficult to calculate the elastic mean free path with good precision [note that for low concentration, Eq. (20) in Sec. V gives the standard expression]. Here, the wavelength is chosen to scale the cutoff radius. Our choice is motivated by the fact that the wavelength is the main quantity playing a role in the behavior of the Hankel functions, which drives the scattering. Zhang and Li[16] also used this quantity to scale their groups of scatterers. Another proof of the complex dependency of cutoff radius on frequency follows in Sec. IV.

TABLE I. Coefficients of surface of cutoff radius calculated for steel cylinders.

c_0	c_1	c_2	c_3	c_4	c_5	c_6	c_7	c_8
1.6	29.0	7.1	−48.8	−72.6	−4.3	29.6	130.5	−81.1

The choice of the threshold $\Delta_E = 10\%$ is arbitrary; other values are, of course, possible. To get a physical meaning for this value, a circular, randomly distributed distribution of 2130 steel cylinders ($\rho_c = 7850\,\mathrm{kg\ m^{-3}}$, $c_L = 5700\,\mathrm{m\ s^{-1}}$, $c_T = 3000\,\mathrm{m\ s^{-1}}$) in water ($c = 1500\,\mathrm{m\ s^{-1}}$, $\rho = 1000\,\mathrm{kg\,m^{-3}}$) is considered. The global concentration is $\phi = 15\%$. A plane wave propagates toward the x-direction (from left to right) with frequency $f = 46.8$ kHz ($ka = 0.2$).

Figures 4(A), 4(B), 4(D), 4(F), and 4(H) show the scattered energy field (in dB) in four cases: Fig. 4(A) shows the exact field (obtained by resolution of the dense problem), and Figs. 4(B), 4(D), 4(F), and 4(H) show three sparse systems, with smaller and smaller cutoff radius [Fig. 4(F) corresponding to the Born approximation case, for which no interaction is taken into account]. Figure 4(B) corresponds to the rate proposed in this work $\Delta_E = 10\%$. All the quantities are reported in Table II.

The considered distribution has a radius of $R_c = 0.1$ m, which corresponds to $100\,a$. This gives a ratio $kR_c = 20$. Considering the cluster cylindrical form, we observe here a scattering behavior similar to the one of a single cylinder scattering at high frequency regime for which most of the energy goes forward. The error on the acoustic fields is represented in Figs. 4(C), 4(E), 4(G), and 4(I). Although Δ_E takes large values, one can observe how weak the error on the field is. This is due to the fact that the error estimator Δ_E includes the error made on the total areas (which are two times bigger than the considered distribution). For both cases Figs. 4(C) and 4(E), the error is almost everywhere below 15 dB, even if $\Delta_E = 22\%$ for case Fig. 4(E). It should be pointed out that the choice of Δ_E can depend on other parameters, for instance, the geometry of the cluster. In our case corresponding to a cylindrical cluster, most of the energy is located on the forward scattering region.

IV. VALIDATION TESTS

This section is devoted to validation cases for which MuScat simulations are compared to other simulations performed using other calculation methods. First, a numerical calculation based on the discontinuous Galerkin method is performed on situations with a few soft cylinders. Then, a comparison with Foldy's model[28] gives very good results, in terms of effective parameters, for low concentration ($\phi = 6\%$) and frequency range $ka \in [0,1]$.

A. Comparison with numerical simulations of the wave equation

Time-domain calculations based on the wave equation are another strategy to investigate multiple scattering

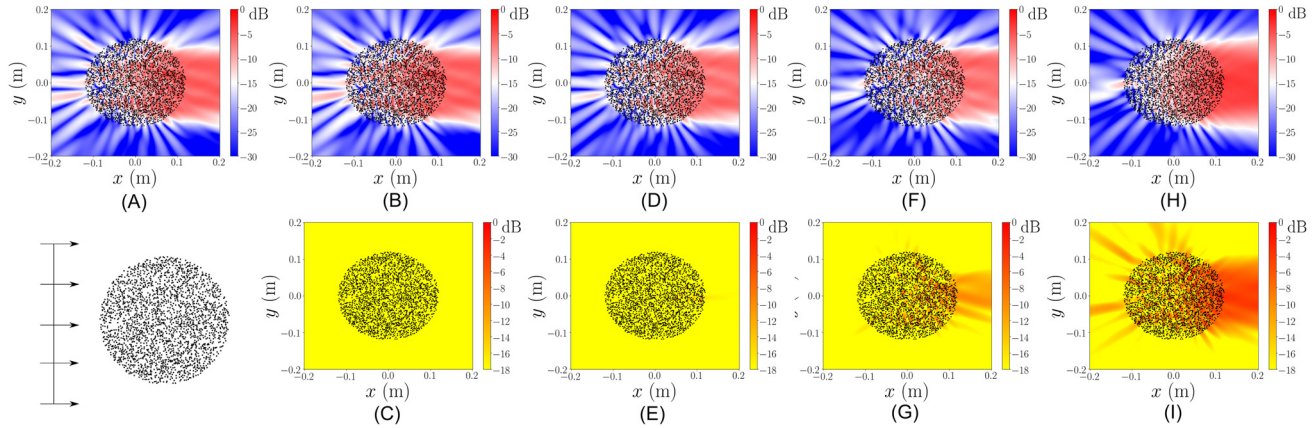

FIG. 4. (Color online) Acoustical energy fields calculated on circular randomly distributed distributions ($\phi = 15\%$, $ka = 0.2$). A plane wave is propagating from left to right. Figures on the top represent the acoustic energy normalized by the maximum of (A). (A) is calculated thanks to the dense system (12), and the others with Eq. (14) with smaller and smaller cutoff radius, reported on Table II. Figures at the bottom represent the energy error introduced by the cutoff radius with respect to (A).

problems. For instance, Pennec *et al.*[29] performed finite difference time domain simulations to study multiplexing and demultiplexing of waves in waveguides. Chekroun *et al.*[30] used a time simulation to compute the effective wave numbers of heterogeneous media in order to compare them with the effective medium theories we listed in the Introduction of this paper. These methods are limited by the number of scatterers due to mesh size limitation. The idea of this section is to compare the scattered field of simple configurations of soft scatterers, calculated by MuScat and the discontinuous Galerkin calculator paradigm.[31,32]

Paradigm is based on time simulation. The source defined in both simulations is a plane wave, and the radius of the cylinders is $a = 1$ mm. Ideal plane waves are never reached in time domain simulations because that means infinite extension. To stay free from diffraction consideration, we decided to compare only the scattered field rather than the total field. Two time simulations have been performed for each case presented here: one with cylinders and the other without (the second one is a free space simulation). In this way, substracting both fields gives the scattered part of the total field. Afterward, a frequency treatment is performed to get the harmonic picture of the field, instead of the time simulation.

Two different configurations are presented here. One is composed of four cylinders placed on the corners of a square, 1 cm × 1 cm. The other is composed of six randomly distributed cylinders. This last case is interesting because cylinders very close to each other are considered.

Figures 5(A) and 5(B) show the scattered fields on two different space lines for two configurations. The space line is represented in green at the top left corner and it is parallel (a) or perpendicular (b) to the propagation direction of the source. The frequency of the source is $ka = 0.7$ for Fig. 5(A) and $ka = 1.06$ for Fig. 5(B). MuScat and paradigm agree with very good precision in both cases. These are the first tests proving the validity of the implemented method.

More than just a validation case, it is also an interesting case of comparison between two different models, one using discretization of elastodynamics equations (paradigm) and the other being only based on acoustical quantities, where the mechanical aspects are all included in the $\mathbb{T}$-matrix of each cylinder.

TABLE II. Energy error for four different cutoff radii D on the same distribution.

D (m)	Δ_E (%)	Percent of interactions	Figures: field, error
0.19	10.0	96.0	(B), (C)
0.15	22.0	77.0	(D), (E)
0.09	49.0	39.0	(F), (G)
0.001	91.0	0.0	(H), (I)

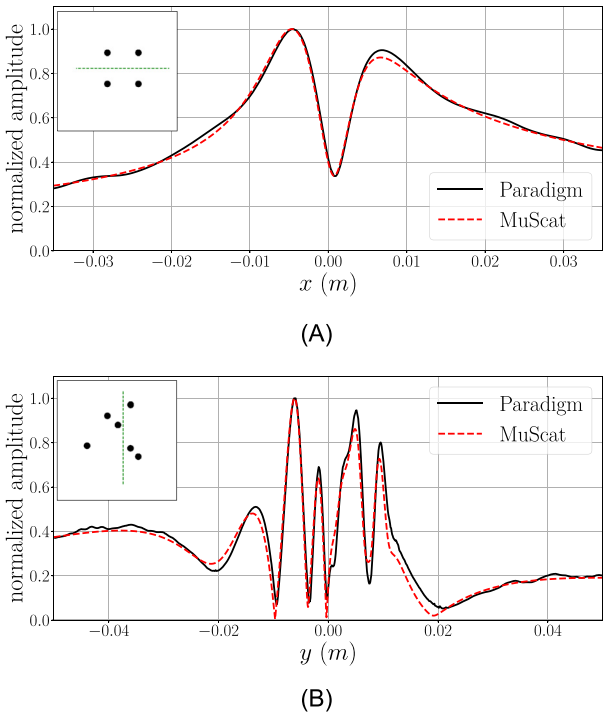

FIG. 5. (Color online) Comparison between the absolute value of the scattered pressure field calculated by discontinuous Galerkin method (black lines) and MuScat (red lines) on a space line represented on green on the top left corner with respect to the positions of the cylinders.

B. Comparison with the independent scattering approximation (ISA)

For low concentrations of scatterers, effective medium theories are often used to calculate the effective celerity and the effective attenuation of the coherent wave through the heterogeneous medium. The idea of the current section is to compare the effective parameters given by Foldy's model and those given by MuScat.

Let us consider a rectangular geometry of size $H \times h$, H being the dimension toward the y axis and h toward the x axis, as presented in Fig. 6. A plane wave is chosen as source and propagates toward the x axis. At position $x = h$, one can write the pressure as

$$\begin{cases} p_0 = Ae^{jkh} & \text{in homogeneous medium,} \\ p_1 = Ae^{jk_{\text{eff}}h} & \text{in heterogeneous medium.} \end{cases} \tag{17}$$

The effective wave number is complex and decomposed as $k_{\text{eff}} = \omega/c_{\text{eff}} + j\alpha_{\text{eff}}$, where α_{eff} is the effective attenuation and c_{eff} is the effective phase velocity. Considering that the phase delay $\arg(p_1/p_0)$ is simply given by $\omega h(1/c_\phi - 1/c_0)$, α_{eff} and c_{eff} are calculated as follows:

$$\begin{cases} \alpha_{\text{eff}} = -\dfrac{1}{h}\ln\left(\left|\dfrac{p_1}{p_0}\right|\right), \\ c_{\text{eff}} = \dfrac{\omega h}{\dfrac{\omega h}{c_\phi} + \arg\left(\dfrac{p_1}{p_0}\right)}. \end{cases} \tag{18}$$

Foldy's model gives an expression for the effective wave number,[7]

$$k_{\text{eff}}^2 = k^2 - 4in_0\sum_n T_n, \tag{19}$$

where n_0 is the number of cylinders by square meter and T_n are the scattering coefficients of one single cylinder. Expressions (18) (used for calculation with MuScat) and (19) are compared numerically.

Calculations with MuScat are performed for randomly distributed distributions of steel cylinders ($\rho_c = 7850\,\text{kg m}^{-3}$, $c_L = 5700\,\text{m s}^{-1}$, $c_T = 3000\,\text{m s}^{-1}$) in water ($c = 1500\,\text{m s}^{-1}$, $\rho = 1000\,\text{kg m}^{-3}$). The concentration is $\phi = 6\%$, which is low enough to consider Foldy's model as a reference. The radius of the cylinders is $a = 400\,\mu\text{m}$. The slab sizes are $H = 60\,\text{cm}$ and $h = 18\,\text{mm}$ (each slab is composed of 1289 cylinders). A plane wave propagates toward the x-direction. To be as close as possible to experimental conditions, the acoustic field is calculated on the surface $H_c = 0.2H$ on which the average is performed. In order to stay free from diffraction considerations (which can occur near the boundaries), the average on 30 different slabs is then calculated instead of moving the measurement line toward the vertical direction. Calculations are performed with $N_m = 3$, which is relevant for the frequency range investigated $0 \le ka \le 1$.

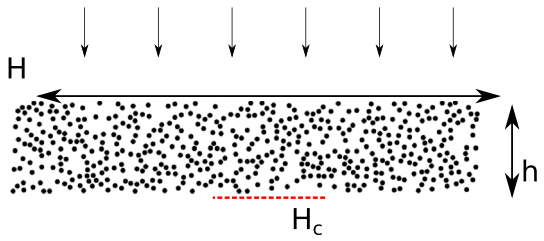

FIG. 6. (Color online) Configuration used to extract effective parameters of random distributions with MuScat.

Figures 7(A) and 7(B) show the dependency of the effective attenuation α_{eff} and phase velocity c_{eff} on frequency. Even if the cylinders (steel cylinders) are more rigid than the host medium (which is water), the effective phase velocity is predicted to be lower than in the host medium for the entire frequency range. Considering the phase velocity as being controlled by a competition between the stiffness of the medium and its density, it is interesting to note here that the effective density increases more than the effective stiffness, which explains why the coherent wave front slows down.

For both parameters, results calculated using the Born approximation are also reported. The Born approximation only gives good results for very low frequencies ($ka < 0.2$).

Otherwise, the agreement is excellent when using the cutoff radius [$D = D(\lambda)$, dark green line] previously calculated. This shows that the surface calculated and presented above can be successfully used in other configurations, which differ by the geometry and the quantities calculated. Considering the $D = 2\lambda$ curve, it is worth noting that the phase velocity does not fit with Foldy's predictions for

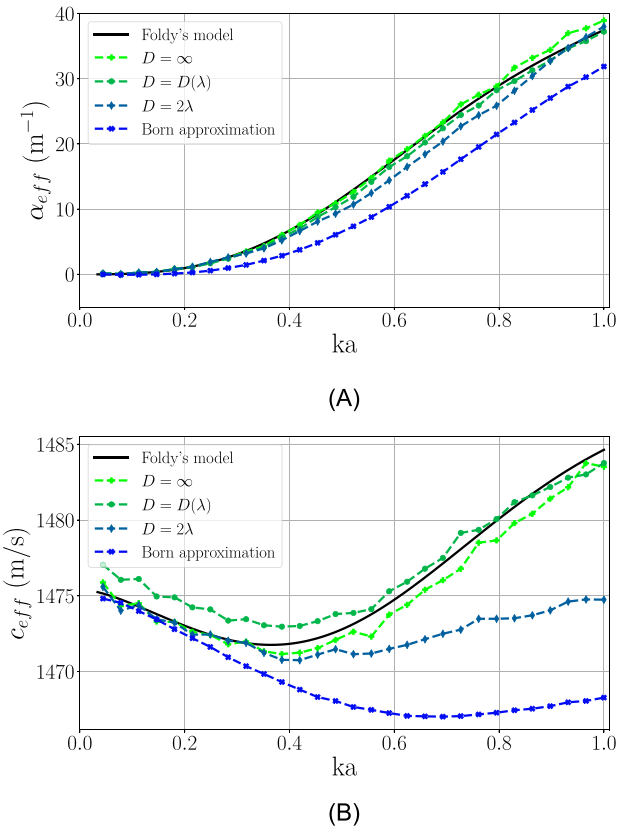

FIG. 7. (Color online) Effective attenuation (A) and phase velocity (B) calculated with MuScat with different cutoff radii.

$ka > 0.5$. This shows that the wavelength dependency can be quite complicated and very different from a linear behavior.

The tests presented in this section clearly show that the implementation is validated for the tested frequencies and concentrations.

V. RANDOMLY DISTRIBUTED MEDIA—COMPARISON BETWEEN AVERAGE PROCESS CALCULATED WITH MUSCAT AND BY HOMOGENIZATION

The main interest of homogenization theories is to compute the effective parameters associated with multiple scattering media, not only the effective wave number, but also density and stiffness.[33] Basically, there are two interests in calculating effective parameters. Either we look for exotic behaviors such as, for example, negative refraction and cloaking, leading to the investigation of acoustic metamaterials, such as those that have appeared on the scene in the last few years.[34] In such cases, we focus on unusual concepts such as negative density and negative compressibility. Or we use the effective parameters to build a homogenized/effective medium, which has the same physical behavior as the multiple scattering medium. This is what was done previously in Sec. IV when the multiple scattering slab was assimilated to an effective slab in order to calculate k_{eff}.

The question in this paper is: Does the assimilation between multiple scattering and effective media carried out with a slab still work for a cluster having another geometry?

It should be noted that k_{eff} is calculated by comparing the two transmission coefficients associated with the multiple scattering and effective media. What about the reflection? Reflection coefficients do not enable this objective to be achieved because the coherence manifests itself through the coherent backscattering, which is another physical phenomenon. Coherent waves result from the average of all the acoustic waves traveling from one cylinder to another in the same direction (that of the incident plane wave), and the coherent backscattering is due to reflected paths that are traveled twice in one or other directions.[35] It should also be noted that, even in transmission, it is not possible to assimilate the multiple scattering transmission coefficient T_{MS} to the effective transmission coefficient T_{eff} if the slab thickness h is greater than the elastic mean free path l_e. This quantity is usually defined by the relation[36]

$$l_e = \frac{1}{2\alpha_{\text{eff}}}. \tag{20}$$

If $h > l_e$, the coherent wave is too attenuated to propagate through the slab and the transmitted field becomes diffusive in nature. Furthermore, if it is well established that $T_{\text{eff}} \approx T_{\text{MS}}$ for $h > l_e$ at normal incidence, this result has never been established at oblique incidence. At oblique incidence, a question remains open: Is there a refraction effect obeying the Snell-Descartes laws at the interface between a homogeneous and a multiple scattering medium? At normal incidence, the wave front of the incident wave coincides with the interface; this is a favorable situation to generate a coherent wave. At oblique incidence, all the waves do not have the same phase reference when they are excited. There is a phase delay that depends on the angle of incidence. In such a case, how is the coherence built? What is the direction of propagation of the coherent wave?

It is these first elements of analysis that led us to consider a multiple scattering cluster more complex than the slab. We have chosen a cluster of cylindrical shape because it has a geometry simple enough to be homogenized and because its radius of curvature is not infinite. It follows that the angle of incidence between the direction of propagation of the incident plane wave and the surface of the cluster range from 0 to $\pi/2$. Moreover, it is expected that the backward and forward scattering reveal different and interesting behaviors. The purpose of this last part is to use the effective parameters in order to compare the wave propagation through the cylindrical multiple scattering cluster and the homogenized one. It is worth noting that similar studies have been investigated by Torrent and Sánchez-Dehesa[37] and Reyes-Ayona *et al.*[38] in the case of cylindrical clusters made up of two-dimensional sonic crystals and in the case of random clusters of cylinders[39] with the idea of identifying effective parameters at low frequencies.

The diameter $D_c = 2R_c$ of the cluster is given in function of the cylinder radius $a = 1$ mm and the elastic mean free path l_e. Two different cases are considered that correspond to the parameters given in Table III. The concentration is $\phi = 10\%$, and the source frequency is fixed at $ka = 0.3$. The concentration is a bit higher than the one considered in Sec. IV but still low enough to consider Foldy's predictions as valid. The physical parameters of the homogenized cylinder are given by $c_L = c_{\text{eff}}$, $\alpha = \alpha_{\text{eff}}$, and $\rho_{\text{eff}} = \phi\rho_c + (1 - \phi)\rho$. For $ka = 0.3$, we have $c_{\text{eff}} = 1454\,\text{m s}^{-1}$, $\alpha_{\text{eff}} = 2.032\,\text{m}^{-1}$, and $\rho_{\text{eff}} = 1690\,\text{kg m}^{-3}$. The effective wave number is given by $k_L = \omega/c_{\text{eff}} + j\alpha_{\text{eff}}$, and the scattering coefficients T_n of the homogenized cluster are the following:

$$T_n = \frac{\dfrac{J_n(kR_c)}{J_n(k_{\text{eff}}R_c)} - \dfrac{\rho_{\text{eff}}kJ_n'(kR_c)}{\rho k_{\text{eff}}J_n'(k_{\text{eff}}R_c)}}{\dfrac{\rho_{\text{eff}}kH_n'^{(1)}(kR_c)}{\rho k_{\text{eff}}J_n'(k_{\text{eff}}R_c)} - \dfrac{H_n^{(1)}(kR_c)}{J_n(k_{\text{eff}}R_c)}}. \tag{21}$$

It is important to note here that the scattering by homogenized clusters falls within the framework of the high frequencies because $kR_c = 36.9$ in the first case ($R_c = l_e/2$) and $kR_c = 123.6$ in the second case ($R_c = 1.675l_e$). The convergence of the modal series requires, therefore, to take into account up to $N_m = 45$ and $N_m = 135$ modes of vibration. This shows that the vibration behavior of clusters can be very complicated due to all the interactions that occur at the microscopic level. For the multiple scattering simulations, the average is performed over 20 different random distributions. We calculate the total scattered energy; the directivity diagrams are

TABLE III. Cluster dimensions considered for the multiple scattering simulations for a concentration $\phi = 10\%$ and frequency of $ka = 0.3$.

	D_c/a	D_c/l_e	N_s	N_m	$N \times N$
(i)	246	1.0	1516	3	7580×7580
(ii)	824	3.35	17020	3	$85\,100 \times 85\,100$

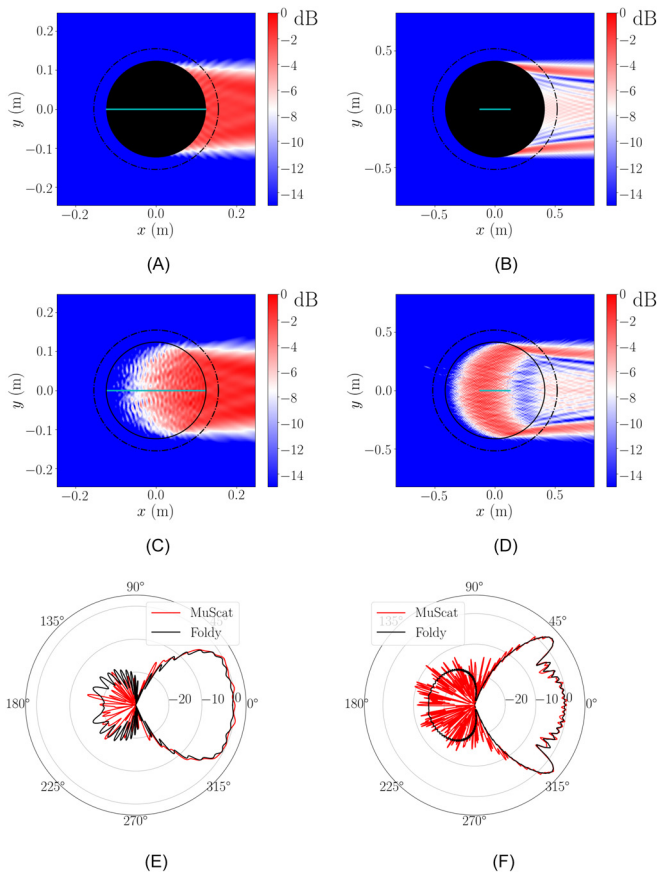

FIG. 8. (Color online) Scattered energy, calculated by homogenization of the heterogeneous medium (A),(B) and MuScat (C),(D). The cylindrical distribution has a radius $R_c = 123a$ (left) or $R_c = 412a$ (right), which correspond to $R_c = l_e/2$ (left) or $R_c = 1.625l_e$ (right). Directivity diagrams (E),(F) are calculated on dotted lines indicated in the figures above. Source is a plane wave propagating from left to right. Cyan lines in the middle indicate the size of l_e.

plotted at a radial distance $l = 1.25R_c$. Normalizations are performed from the maximum of energy given by MuScat simulations, and the dynamic range is fixed at -15 dB [except for Fig. 9(A) for which it is -30 dB].

Figure 8 shows results for an incident plane wave propagating from left to right. In Figs. 8(C) and 8(D) the construction of coherent waves resulting from the averaging process appears very clearly. The averaging process is fully effective only from a certain distance away from the boundary of the cylindrical cluster, which is enlightened by the incident plane wave. The place where the coherent wave is generated describes a semi-circle and makes a boundary layer appear on the left side of the cluster, where the multiple scattering is not coherent. This effect, which has already been discussed by Linton and Martin,[20] could be quantified from simulations by MuScat.

In Figs. 8(A) and 8(C), for which the diameter is equal to the elastic mean free path, the coherent wave seems to propagate through the cluster as a bulk wave. Figures 8(A) and 8(C) show a broadly satisfactory agreement between homogenized and numerical simulations. However, if Fig. 8(E) shows a very good agreement in forward scattering, the situation is very different for the backward scattering. This difference can be explained in a fairly simple way. The homogenized simulation assumes that the coherent wave occupies the whole cluster, which is not the case since we have brought to light the existence of a boundary layer (close to the reflection) where the multiple scattering is not coherent. It should also be noted that the forward scattering is very strong, more than 15 dB higher than the backscattering.

In Figs. 8(B) and 8(D), the elastic mean free path l_e is much smaller than the cluster diameter. As shown in Fig. 8(D), the coherent wave is attenuated before reaching the opposite side of the cluster. In this case, we expect to see a difference between homogenized and numerical simulations, even in forward scattering. Surprisingly, this is not what is observed in Fig. 8(F), where the agreement is excellent in forward scattering. In this case, the coherent wave does not propagate through the cluster, as previously studied, but around the cluster. It seems that coherent waves follow the cluster curvature in a clockwise and anticlockwise direction. Can we talk about surface coherent waves? We do not really have a way of analyzing this surface phenomenon, but we can choose another source in order to verify whether or not it still exists.

Figure 9 shows results for a point source located on the axis $y = 0$ at a distance of $1.1R_c$ on the left of the cluster. The elastic mean free path l_e is much smaller than the cluster diameter. The previous result is fully confirmed, Figs. 9(A) and 9(B) show that most of the energy is radiated from the boundary of the cluster. Homogenized and multiple scattering models seem to give the same results, but even if the directivity patterns have the same shape, a difference of approximately 10 dB is visible on all directions in directivity diagrams [cf. Fig. 9(C)]. This difference can be explained by the fact that the wave front of the coherent wave is cylindrical, as we can see in Fig. 9(B). So the wave number of the homogenized cluster, which is calculated for a coherent

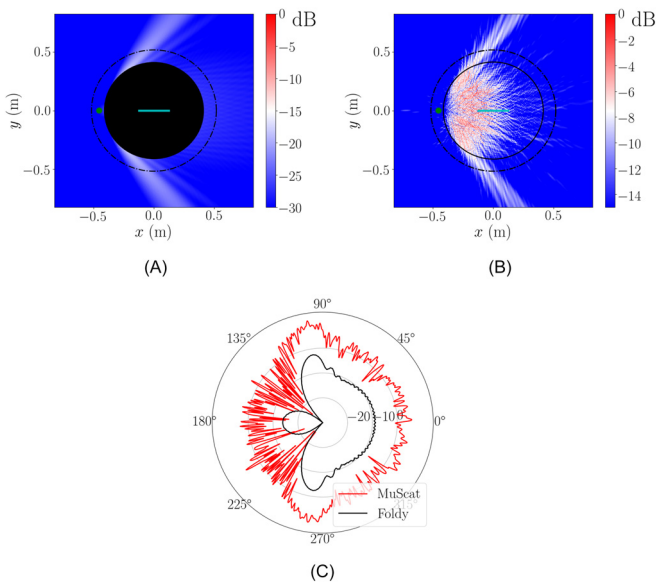

FIG. 9. (Color online) Scattered energy, calculated by homogenization of the heterogeneous medium (A) and MuScat (B). The cylindrical distribution has a radius $R_c = 412a$, which correspond to $R_c = 6.7l_e$. Directivity diagram (C) is calculated on dotted lines and indicated on figures above. Source is a point source located on position $(1.1R_c,0)$ (green point). Cyan lines in the middle indicate the size of l_e.

wave with a plane wave front, is probably not well adapted to the situation.

In conclusion, all the results show that homogenization theories are not fully adapted in order to describe the multiple scattering by a cluster of cylindrical shape. In particular, the backward scattering is far from being well described. However, the forward scattering seems always to yield good results if the incident wave is a plane wave, whatever the value of the elastic mean free path compared to the cylindrical cluster diameter.

VI. CONCLUSION

We have implemented an innovative resolution method to treat the multiple scattering of sound in 2D. Our resolution method can deal with any situation with many randomly distributed cylinders, combining numerous different $\mathbb{T}$-matrices and a very large number of cylinders. We have shown applications with matrices of sizes bigger than 80 000 $\times$ 80 000 for random positions. The scalability of the resolution method allows us to think about considering much bigger problems. The next step of this work will deal with generalizing this method in three dimensions, and efforts will be concentrated on comparison with experimental data.

ACKNOWLEDGMENTS

The authors wish to thank Ph.D. student Pierre Massé [Sciences et Technologies de la Musique et du Son (STMS)–Institut de Recherche et Coordination Acoustique/Musique (IRCAM)] for his careful reading of this manuscript.

[1]F. Zàviška, "über die Beugung elektromagnetischer Wellen an parallelen, unendlich langen Kreiszylindern," Ann. Phys. **345**, 1023–1056 (1913).
[2]S. Bose and A. Mal, "Longitudinal shear waves in a fiber-reinforced composite," Int. J. Solids Struct. **9**, 1075–1085 (1973).
[3]M. Lax, "Multiple scattering of waves. II. The effective field in dense systems," Phys. Rev. **85**, 621–629 (1952).
[4]V. K. Varadan, V. V. Varadan, and Y. Pao, "Multiple scattering of elastic waves by cylinders of arbitrary cross section. I. SH waves," J. Acoust. Soc. Am. **63**, 1310–1319 (1978).
[5]P.-Y. Le Bas, F. Luppé, J.-M. Conoir, and H. Franklin, "*N*-shell cluster in water: Multiple scattering and splitting of resonances," J. Acoust. Soc. Am. **115**, 1460–1467 (2004).
[6]C. M. Linton and P. A. Martin, "Multiple scattering by random configurations of circular cylinders: Second-order corrections for the effective wavenumber," J. Acoust. Soc. Am. **117**, 3413–3423 (2005).
[7]A. N. Norris and J.-M. Conoir, "Multiple scattering by cylinders immersed in fluid: High order approximations for the effective wavenumbers," J. Acoust. Soc. Am. **129**, 104–113 (2011).
[8]G. O. Olaofe, "Scattering by two cylinders," Radio Sci. **5**, 1351–1360, https://doi.org/10.1029/RS005i011p01351 (1970).
[9]J. W. Young and J. C. Bertrand, "Multiple scattering by two cylinders," J. Acoust. Soc. Am. **58**, 1190–1195 (1975).
[10]R. P. Radlinski and T. J. Meyers, "Radiation patterns and radiation impedances of a pulsating cylinder surrounded by a circular cage of parallel cylindrical rods," J. Acoust. Soc. Am. **56**, 842–848 (1974).
[11]F. A. Amirkulova and A. N. Norris, "Acoustic multiple scattering using recursive algorithms," J. Comput. Phys. **299**, 787–803 (2015).
[12]L. Greengard and V. Rokhlin, "A fast algorithm for particle simulations," J. Comput. Phys. **73**(2), 325–348 (1987).
[13]S. Koc and W. C. Chew, "Calculation of acoustical scattering from a cluster of scatterers," J. Acoust. Soc. Am. **103**, 721–734 (1998).
[14]N. A. Gumerov and R. Duraiswami, "Computation of scattering from clusters of spheres using the fast multipole method," J. Acoust. Soc. Am. **117**, 1744–1761 (2005).
[15]N. A. Gumerov and R. Duraiswami, *Fast Multipole Methods for the Helmholtz Equation in Three Dimensions* (Elsevier, Oxford, UK, 2004).
[16]Y. J. Zhang and E. P. Li, "Fast multipole accelerated scattering matrix method for multiple scattering of a large number of cylinders," Prog. Electromagn. Res. **72**, 105–126 (2007).
[17]S. Balay, S. Abhyankar, M. F. Adams, J. Brown, P. Brune, K. Buschelman, L. Dalcin, A. Dener, V. Eijkhout, W. D. Gropp, D. Kaushik, M. G. Knepley, D. A. May, L. C. McInnes, R. T. Mills, T. Munson, K. Rupp, P. Sanan, B. F. Smith, S. Zampini, H. Zhang, and H. Zhang, PETSc, available at http://www.mcs.anl.gov/petsc (Last viewed May 1, 2019).
[18]S. Balay, S. Abhyankar, M. F. Adams, J. Brown, P. Brune, K. Buschelman, L. Dalcin, A. Dener, V. Eijkhout, W. D. Gropp, D. Kaushik, M. G. Knepley, D. A. May, L. C. McInnes, R. T. Mills, T. Munson, K. Rupp, P. Sanan, B. F. Smith, S. Zampini, H. Zhang, and H. Zhang, "PETSc users manual," Technical Report No. ANL-95/11—Revision 3.10, Argonne National Laboratory (2012).
[19]S. Balay, W. D. Gropp, L. C. McInnes, and B. F. Smith, "Efficient management of parallelism in object oriented numerical software libraries," in *Modern Software Tools in Scientific Computing*, edited by E. Arge, A. M. Bruaset, and H. P. Langtangen (Birkhäuser, Basel, Switzerland, 1997), pp. 163–202.
[20]P. Martin, *Multiple Scattering—Interaction of Time-Harmonic Waves with N Obstacles* (Cambridge University Press, Cambridge, UK, 2006).
[21]J. J. Faran, "Sound scattering by solid cylinders and spheres," J. Acoust. Soc. Am. **23**(4), 405–418 (1951).
[22]N. D. Veksler, *Resonance Acoustic Spectroscopy* (Springer, Berlin, 1993).
[23]X. Antoine, C. Chniti, and K. Ramdani, "On the numerical approximation of high-frequency acoustic multiple scattering problems by circular cylinders," J. Comput. Phys. **227**, 1754–1771 (2008).
[24]T. Valier-Brasier and J.-M. Conoir, "Resonant acoustic scattering by two spherical bubbles," J. Acoust. Soc. Am. **145**, 301–311 (2019).
[25]N. Gould and J. Scott, "The state-of-the-art of preconditioners for sparse linear least-squares problems," ACM Trans. Math. Softw. **43**, 1–35 (2017).
[26]I. S. Duff, "The impact of high-performance computing in the solution of linear systems: Trends and problems," J. Comput. Appl. Math. **123**, 515–530 (2000).
[27]S. Biwa, S. Yamamoto, F. Kobayashi, and N. Ohno, "Computational multiple scattering analysis for shear wave propagation in unidirectional composites," Int. J. Solids Struct. **41**, 435–457 (2004).
[28]L. L. Foldy, "The multiple scattering of waves. I. General theory of isotropic scattering by randomly distributed scatterers," Phys. Rev. **67**, 107–119 (1945).
[29]Y. Pennec, B. Djafari-Rouhani, J. O. Vasseur, A. Khelif, and P. A. Deymier, "Tunable filtering and demultiplexing in phononic crystals with hollow cylinders," Phys. Rev. E **69**, 046608 (2004).
[30]M. Chekroun, L. L. Marrec, B. Lombard, and J. Piraux, "Multiple scattering of elastic waves: A numerical method for computing the effective wavenumbers," Waves Random Complex Media **22**, 398–422 (2012).
[31]B. Tripathi, A. Luca, S. Baskar, F. Coulouvrat, and R. Marchiano, "Element centered smooth artificial viscosity in discontinuous Galerkin method for propagation of acoustic shock waves on unstructured meshes," J. Comput. Phys. **366**, 298–319 (2018).
[32]A. Luca, R. Marchiano, and J.-C. Chassaing, "Numerical simulation of transit-time ultrasonic flowmeters by a direct approach," IEEE Trans. Ultrason. Ferroelec. Freq. Control **63**(6), 886–897 (2016).
[33]C. Aristégui and Y. C. Angel, "Effective mass density and stiffness derived from *p*-wave multiple scattering," Wave Motion **44**, 153–164 (2007).
[34]M. R. Haberman and A. Norris, "Acoustic metamaterials," Acoust. Today **12**, 31–39 (2016).
[35]A. Aubry, A. Derode, P. Roux, and A. Tourin, "Coherent backscattering and far-field beamforming in acoustics," J. Acoust. Soc. Am. **121**, 70–77 (2007).
[36]A. Derode, V. Mamou, and A. Tourin, "Influence of correlations between scatterers on the attenuation of the coherent wave in a random medium," Phys. Rev. E **74**, 036606 (2006).
[37]D. Torrent and J. Sánchez-Dehesa, "Sound scattering by anisotropic metafluids based on two-dimensional sonic crystals," Phys. Rev. B **79**, 174104 (2009).
[38]E. Reyes-Ayona, D. Torrent, and J. Sánchez-Dehesa, "Homogenization theory for periodic distributions of elastic cylinders embedded in a viscous fluid," J. Acoust. Soc. Am. **132**, 2896–2908 (2012).
[39]D. Torrent and J. Sánchez-Dehesa, "Effective parameters of clusters of cylinders embedded in a nonviscous fluid or gas," Phys. Rev. B **74**, 224305 (2006).